nature neuroscience

Brief Communication

https://doi.org/10.1038/s41593-023-01272-0

Developmental trajectory of transmission speed in the human brain

Received: 17 March 2022

Accepted: 9 February 2023

Published online: 9 March 2023

Check for updates

Dorien van Blooijs[1,2,3,5], Max A. van den Boom[1,4,5], Jaap F. van der Aar[2], Geertjan M. Huiskamp[2], Giulio Castegnaro[2], Matteo Demuru[2], Willemiek J. E. M. Zweiphenning[2], Pieter van Eijsden[2], Kai J. Miller[4], Frans S. S. Leijten[2] & Dora Hermes[1]

The structure of the human connectome develops from childhood throughout adolescence to middle age, but how these structural changes affect the speed of neuronal signaling is not well described. In 74 subjects, we measured the latency of cortico-cortical evoked responses across association and U-fibers and calculated their corresponding transmission speeds. Decreases in conduction delays until at least 30 years show that the speed of neuronal communication develops well into adulthood.

The development of rapid communication between human brain regions is essential for cognitive function. The speed of neuronal transmission is fundamental to the temporal organization of neuronal activity[1] and is a core component in many computational human brain models[2]. The developing axons in the human brain support rapid neuronal transmission, influencing whether electrical signals arrive at the same or at different times and shaping the timescales of functional connectivity[3]. However, little is known about the maturation process of transmission speed in the human brain, partially because the axonal diameter in the adult human brain is relatively large compared with most other mammalian species[4].

Anatomical studies indicate that the structural human connectome follows a long developmental trajectory: postmortem studies have shown that myelination starts in the late prenatal period and continues into late adolescence[5]. Magnetic resonance imaging (MRI) analyses have demonstrated that white matter properties change across the life-span[6], often reaching a plateau around 30 years of age.

However, electroencephalography and magnetoencephalography studies that approximate transmission speed by measuring the latency of visual evoked potentials, show highly variable ages at which development plateaus. While studies consistently find decreases in the latency of the visual evoked potential at around 100 ms during infancy and early childhood (<13 years)[7–9], the developmental plateau at which latency decreases change to latency increases differs across studies. Some studies report that evoked potential latency starts increasing after age 13 (ref. [10]), others report no change in latency during adolescence[11,12], others report that latency decreases up to age 20 followed by an increase[13–15], while others report that latency decreases up to age 40 years[16,17] (Supplementary Table 2). One cortico-cortical evoked potential (CCEP) study reported that conduction delays in subjects older than 15 years were only 1 ms faster compared with younger subjects[18]. This poses the question of whether the long structural maturation process translates to changes in neuronal transmission speed.

To characterize the maturation process of transmission speed in the human brain, we measured single-pulse-stimulation-evoked CCEPs during human intracranial electrocorticography (ECoG) recordings in a large group of 74 subjects aged 4–51 years old. CCEPs often show an early surface negative deflection (N1) within 100 ms after stimulating another electrode pair. Figure 1b shows an example of how the N1 response measured in frontal areas upon parietal stimulation peaks around 45 ms in three young subjects (aged 4, 7 and 8 years), while peaking around 1.5–2 times faster—around 25–30 ms—in three older subjects (aged 26, 34 and 35 years).

This rapid negative N1 potential measured with ECoG on the brain surface has been related to direct cortico-cortical white matter connections[19], and is thought to be generated by synchronized, excitatory synaptic activation of the distal layer apical dendrites of the pyramidal cells[20]. While this feature selection likely ignores many other aspects of the evoked potential that provide a richer characterization of cortico-cortical communication[21], the N1 response provides insight into transmission speed across several bundles in the human white matter connectome[18,22].

[1]Department of Physiology and Biomedical Engineering, Mayo Clinic, Rochester, MN, USA. [2]Department of Neurology and Neurosurgery, UMC Utrecht Brain Center, University Medical Center Utrecht, Utrecht, the Netherlands. [3]Stichting Epilepsie Instellingen Nederland (SEIN), Zwolle, the Netherlands. [4]Department of Neurosurgery, Mayo Clinic, Rochester, MN, USA. [5]These authors contributed equally: Dorien van Blooijs, Max A. van den Boom.
e-mail: hermes.dora@mayo.edu

https://doi.org/10.1038/s41593-023-01272-0

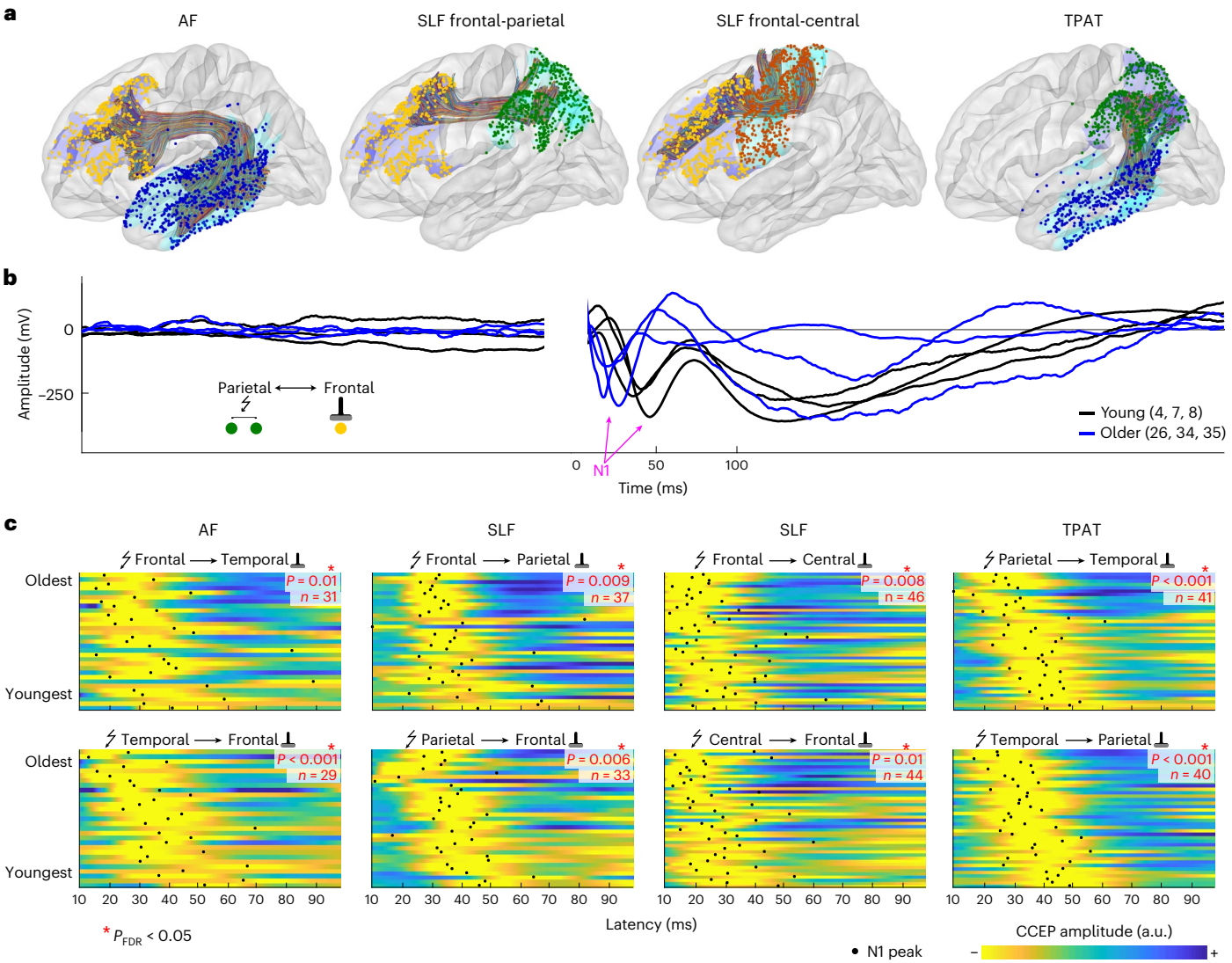

Fig. 1 | Electrode positions, fiber tracts and evoked potentials. a, MNI brain surface showing white matter tracts and electrode positions at endpoints from all 74 subjects. **b**, CCEPs from young subjects (black lines, 4, 7 and 8 years old) and older subjects (blue lines, 26, 34 and 35 years old) across the SLF frontal-parietal tract after parietal stimulation. The N1 peak is indicated by a magenta arrow. **c**, CCEP responses for all subjects and their N1 peak latency (black dots), organized by age for each white matter tract and direction. CCEPs are unit length normalized and yellow indicates the largest negative deflection. A red asterisk indicates a significant negative correlation between age and N1 latency (Spearman's ρ, two-sided, $P < 0.05$, FDR correction for multiple comparisons). The statistical values from left to right, top to bottom are: $\rho = -0.43$, $P = 0.01$, $n = 31$; $\rho = -0.43$, $P = 0.009$, $n = 37$; $\rho = -0.40$, $P = 0.008$, $n = 46$; $\rho = -.64$, $P < 0.001$, $n = 41$; $\rho = -0.62$, $P < 0.001$, $n = 29$; $\rho = -0.48$, $P = 0.006$, n = 33; $\rho = -0.37$, $P = 0.01$, $n = 44$; $\rho = -0.61$, $P < 0.001$, $n = 40$.

To quantify age-related changes in conduction delays across some well described association fiber bundles, we use a white matter atlas to extract CCEPs across the arcuate fasciculus (AF), two sections of superior longitudinal fasciculus (SLF) and the temporo-parietal aslant tract (TPAT) in each subject[23] (Fig. 1a). The SLF was segmented into frontal-parietal and frontal-central connections given the different lengths of these segments. We find that N1 latency correlates negatively with age across all four pathways (Fig. 1c; Spearman's ρ, $P_{FDR} < 0.05$). We note that the number of CCEPs does not change consistently with age, indicating no age-related changes in the overall level of connectivity (Supplementary Fig. 2). The latency decreases show that conduction delays across association fibers in the human brain decrease with development.

We then describe the maturation process across these association fibers by fitting a first- and second-order polynomial model where age predicts N1 latency (Fig. 2). These models have been used before in MRI studies of development[6,24]. A robust regression and leave-one-out cross-validation further ensures that single subjects do not drive the results and lets the data indicate which connections are better described by a linear or quadratic model. N1 latency is well predicted by age in the AF, frontal-parietal SLF, frontal to central SLF and TPAT. Moreover, conduction delays mature well into adulthood. Before the age of 10 years, latency decreases by around 0.73 ms per year on average, while between age 20 and 30 years, latency decreases less rapidly by around 0.43 ms per year on average. The quadratic models indicate that a minimum latency of around 25 ms was reached after age 30 years. These small, yearly changes in conduction delays translate in an increase in transmission speed from childhood (6–13 years) to adulthood (19–64 years) of around twofold from roughly 1.5–3 m s^{-1} to 3–6 m s^{-1} (Fig. 2). This indicates that the development of rapid transmission speed across long-range association fibers matures well throughout adolescence.

Short-range connections across neighboring gyri such as the pre- and postcentral gyrus and within frontal and parietal regions are supported by U-fibers. Latencies decrease significantly with age across

https://doi.org/10.1038/s41593-023-01272-0

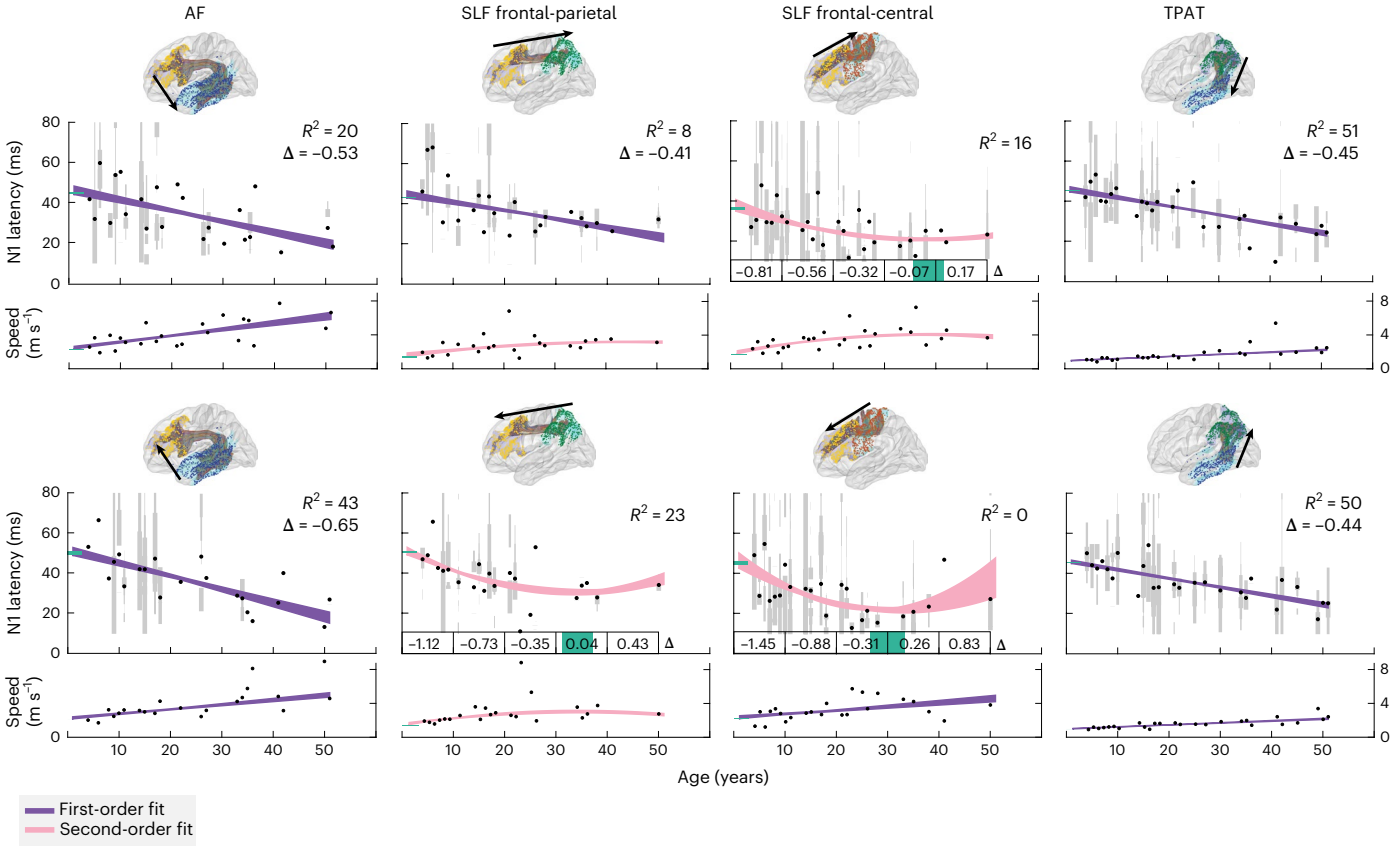

Fig. 2 | Developmental trajectory of conduction delay and speed across long-range connections. Average transmission latency and speed estimated by the N1 component for the AF, frontal-parietal SLF, frontal-central SLF and TPAT (left to right). Gray bars show distributions within each subject, the bar width scales with the number of measured responses. Black dots show N1 latency or speed averaged across subjects of the same age. First- and second-order polynomial models (fit with robust regression and shown with 95% confidence intervals) explain the changes in N1 latency or speed as a function of age. The coefficient of determination (R^2) indicates the variance in latency explained by age (compared with a mean latency rather than a zero baseline). The R^2 is calculated with leave-one-out cross-validation and used to indicate whether the first-order (purple) or second-order (pink) polynomial model explained more variance in the data. For second-order polynomial model fits, the 95% confidence interval is shown in green for the minimum age on the *x* axis and for the N1 latency intercept on the *y* axis. For the first-order polynomial fits, insets show the slope change (Δ) in milliseconds per year. For the second-order polynomial fits, the slope change is displayed in milliseconds per year averaged across 10 years of age. The sample sizes (n = number of ages) for the top row are: 23, 23, 27 and 26 (from left to right), and 21, 22, 23 and 26 (from left to right) for the bottom row.

these short connections (Fig. 3a,b), with corresponding increases in speed (Fig. 3c). U-fibers overall reached speeds up to around 2 m s^{-1}. The model fits show that latencies decrease until age 35 years or older, indicating that transmission speeds across U-fibers mature well throughout adolescence. Interestingly, the frontal and parietal U-fibers had longer latencies during early childhood (>40 ms) compared with the central U-fibers. This is consistent with the idea that sensorimotor regions mature before frontal and parietal association areas[25].

While the overall developmental trajectory of the U-fibers was comparable with that of association fibers there were also important differences. The latencies across the longest association fibers (AF and parietal-frontal SLF) during childhood range from around 45 to 55 ms (Fig. 2), while the childhood latencies of central U-fibers range from around 30 to 40 ms (Fig. 3b). However, at adulthood, latencies of 20–30 ms are typical for both association and central U-fibers. The maximum speeds reached across the U-fibers (around 2–3 m s^{-1}) are therefore smaller compared with the longer range association fibers (around 3–6 m s^{-1}). Axon diameters show large variations ranging from 0.16 to 9 µm in the human brain and, given the limitations of the cranial space, only a small number of large axons can have a larger diameter[1,4]. In myelinated axons, the conduction velocity increases approximately linearly with axon diameter[26]. Smaller U-fiber axons compared with larger association fiber axons may explain the slower speeds in the U-fibers.

The data reveal variability within and between the subjects. Some variability can probably be attributed to a heterogeneous subject population with different axonal properties and noise levels. Other variability may be explained by the fact that, in many natural processes, increases in the mean are related to increases in variability (such as firing rates typically following a Poisson distribution[27]). We indeed find that slower N1 responses often had increased variance (Supplementary Fig. 4) and increased widths (Supplementary Fig. 5), while we found no evidence for a relation between subject's age and variance in latency (Supplementary Fig. 3). This indicates that faster cortico-cortical connections allow for overall more precise timing, whereas timing is less precise in slower cortico-cortical connections.

Our data indicate that transmission speeds are still maturing during adolescence and early adulthood. Many psychopathologies, like schizophrenia, anxiety disorders, depression and bipolar disorders, can emerge during these periods[28], emphasizing the potential importance of our findings for these diseases. We note that, while our subjects suffered from epilepsy, there were no consistent effects of the seizure onset region on latency (Supplementary Figs. 6 and 7), and epilepsy may merely have added noise to the estimates. The large number of subjects allows us to establish a normative baseline with which different pathologies may be compared.

https://doi.org/10.1038/s41593-023-01272-0

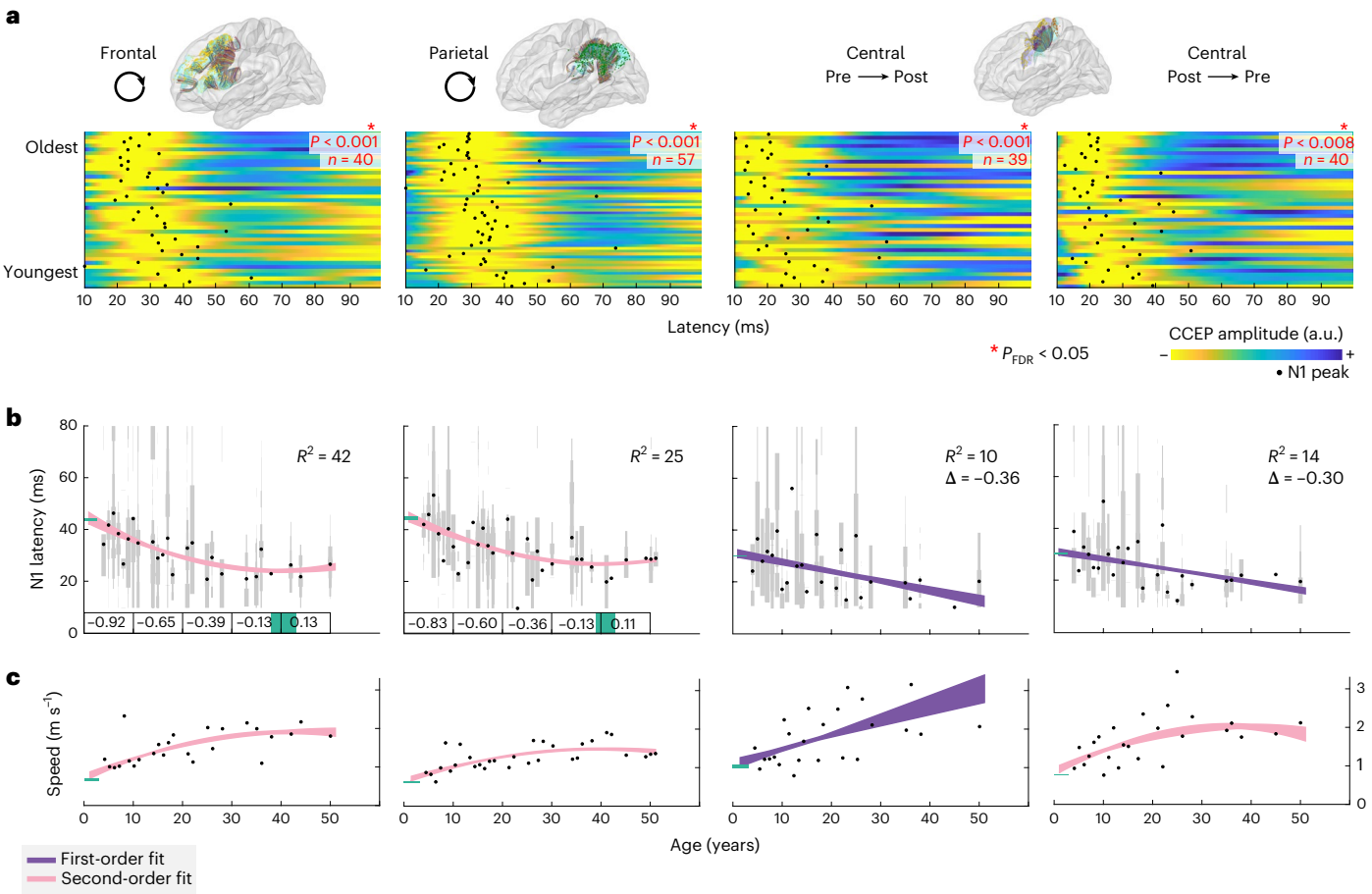

Fig. 3 | Short-range connections decrease in conduction delay with age. **a**, The CCEP responses and their N1 peak latencies (black dots) ordered by age for atlas-based U-fiber connections on frontal, parietal, pre- to postcentral and post- to precentral regions. CCEPs are unit length normalized and yellow indicates the largest negative deflection. A red asterisk indicates a significant negative correlation between age and N1 latency (Spearman's ρ, two-sided test, FDR-corrected, $P_{FDR} < 0.05$). The statistical values from left to right and the number of subjects n are: $\rho = -0.55$, $P < 0.001$, $n = 40$; $\rho = -0.53$, $P < 0.001$, $n = 57$; $\rho = -0.53$, $P < 0.001$, $n = 39$; $\rho = -0.43$, $P = 0.008$, $n = 40$. **b**, Average conduction delays estimated by the N1 latency. Gray bars show distributions within each subject, bar width scales with the number of measured responses. Black dots show N1 latency averaged across subjects of the same age. First- and second-order polynomial models (shown with 95% confidence interval) explain the changes in N1 latency as a function of age. The sample sizes (number of ages) are 25, 32, 25 and 25 from left to right. Explained variance (R^2) calculated with leave-one-out cross-validation indicates whether the first-order (purple) or second-order (pink) polynomial model explains more variance. For all model fits, the 95% confidence interval of the N1 latency intercept (latency at the youngest age) is shown in green on the y axis. For the first-order polynomial fits, insets show the slope change (Δ) in milliseconds per year. For second-order polynomial model fits, the 95% confidence interval of the minimum age is shown in green on the x axis and the slope change is displayed in milliseconds per year averaged across 10 years of age. **c**, Same as **b** for transmission speed based on the average U-fiber length (m s^{-1}) and the same sample sizes.

A long maturation process of transmission speed aligns with findings from noninvasive neuroimaging studies that show that association white matter pathways in the human brain mature well into early adulthood[24,29,30]. MRI studies of the white matter pathways have captured some of these processes and show that white matter development follows a quadratic function with a peak between 30 and 40 years of age[6,31]. This trajectory is comparable with the developmental trajectory of conduction delay that is shown in our data. While this long developmental trajectory is consistent with some evoked potential studies[16,17], other early sensory evoked potentials may show a much faster developmental trajectory until the age of about 20 years[10,13–15]. Some of the variability between evoked potential studies may stem from the development of intermediate synapses between the sensory input and brain measurements. Alternatively, the fast development of some early sensory evoked potentials could also be related to the fact that projection fibers to sensory regions develop faster compared with association fibers[24,29]. Sensory evoked potentials that spread across projection fibers to sensory regions may mature more rapidly compared with the stimulation-evoked potentials across the association fibers measured in the current study.

A simple characterization of the timing of direct cortico-cortical interactions has large implications for the temporal dynamics of brain function. Neuronal synchrony depends on the precise timing, and development can therefore either benefit or deteriorate synchronized brain activity[1]. Twofold increases in the speed of transmission were observed in long-range as well as short-range connections in the human brain. The large, consistent effects of age on transmission speed in our measurements provide normative estimates for the timescales of cortico-cortical signaling in distributed as well as local human brain networks.

Online content

Any methods, additional references, Nature Portfolio reporting summaries, source data, extended data, supplementary information, acknowledgements, peer review information; details of author contributions and competing interests; and statements of data and code availability are available at https://doi.org/10.1038/s41593-023-01272-0.

References

1. Buzsáki, G., Logothetis, N. & Singer, W. Scaling brain size, keeping timing: evolutionary preservation of brain rhythms. *Neuron* **80**, 751–764 (2013).
2. Neymotin, S. A. et al. Human Neocortical Neurosolver (HNN), a new software tool for interpreting the cellular and network origin of human MEG/EEG data. *eLife* **9**, e51214 (2020).
3. Honey, C. J., Kötter, R., Breakspear, M. & Sporns, O. Network structure of cerebral cortex shapes functional connectivity on multiple time scales. *Proc. Natl Acad. Sci. USA* **104**, 10240–10245 (2007).
4. Wang, S. S.-H. et al. Functional trade-offs in white matter axonal scaling. *J. Neurosci.* **28**, 4047–4056 (2008).
5. Paus, T. Growth of white matter in the adolescent brain: myelin or axon?. *Brain Cogn.* **72**, 26–35 (2010).
6. Yeatman, J. D., Wandell, B. A. & Mezer, A. A. Lifespan maturation and degeneration of human brain white matter. *Nat. Commun.* **5**, 4932 (2014).
7. Barnet, A. B. et al. VEP development in infancy and early childhood. A longitudinal study. *Electroencephalogr. Clin. Neurophysiol.* **49**, 476–489 (1980).
8. Taylor, M. J. & McCulloch, D. L. Visual evoked potentials in infants and children. *J. Clin. Neurophysiol.* **9**, 357–372 (1992).
9. Onofrj, M., Thomas, A., Iacono, D., D'Andreamatteo, G. & Paci, C. Age-related changes of evoked potentials. *Neurophysiol. Clin.* **31**, 83–103 (2001).
10. Sokol, S., Moskowitz, A. & Towle, V. L. Age-related changes in the latency of the visual evoked potential: influence of check size. *Electroencephalogr. Clin. Neurophysiol.* **51**, 559–562 (1981).
11. Mahajan, Y. & McArthur, G. Maturation of visual evoked potentials across adolescence. *Brain Dev.* **34**, 655–666 (2012).
12. Stockard, J. J., Hughes, J. F. & Sharbrough, F. W. Visually evoked potentials to electronic pattern reversal: latency variations with gender, age, and technical factors. *Am. J. EEG Technol.* **19**, 171–204 (1979).
13. Allison, T., Hume, A. L., Wood, C. C. & Goff, W. R. Developmental and aging changes in somatosensory, auditory and visual evoked potentials. *Electroencephalogr. Clin. Neurophysiol.* **58**, 14–24 (1984).
14. Caffarra, S. et al. Development of the visual white matter pathways mediates development of electrophysiological responses in visual cortex. *Hum. Brain Mapp.* **42**, 5785–5797 (2021).
15. Armstrong, R. A., Slaven, A. & Harding, G. F. Visual evoked magnetic fields to flash and pattern in 100 normal subjects. *Vis. Res.* **31**, 1859–1864 (1991).
16. Tobimatsu, S., Kurita-Tashima, S., Nakayama-Hiromatsu, M., Akazawa, K. & Kato, M. Age-related changes in pattern visual evoked potentials: differential effects of luminance, contrast and check size. *Electroencephalogr. Clin. Neurophysiol.* **88**, 12–19 (1993).
17. Shaw, N. A. & Cant, B. R. Age-dependent changes in the latency of the pattern visual evoked potential. *Electroencephalogr. Clin. Neurophysiol.* **48**, 237–241 (1980).
18. Lemaréchal, J.-D. et al. A brain atlas of axonal and synaptic delays based on modelling of cortico-cortical evoked potentials. *Brain* **145**, 1653–1667 (2022).
19. Matsumoto, R. et al. Functional connectivity in the human language system: a cortico-cortical evoked potential study. *Brain* **127**, 2316–2330 (2004).
20. Mitzdorf, U. Current source-density method and application in cat cerebral cortex: investigation of evoked potentials and EEG phenomena. *Physiol. Rev.* **65**, 37–100 (1985).
21. Miller, K. J., Müller, K.-R. & Hermes, D. Basis profile curve identification to understand electrical stimulation effects in human brain networks. *PLoS Comput. Biol.* **17**, e1008710 (2021).
22. Keller, C. J. et al. Rhythm in joint action: psychological and neurophysiological mechanisms for real-time interpersonal coordination. *Philos. Trans. R. Soc. Lond. B Biol. Sci.* **369**, 1653 (2014).
23. Yeh, F.-C. Population-based tract-to-region connectome of the human brain and its hierarchical topology. *Nat. Commun.* **13**, 4933 (2022).
24. Lebel, C., Treit, S. & Beaulieu, C. A review of diffusion MRI of typical white matter development from early childhood to young adulthood. *NMR Biomed.* **32**, e3778 (2019).
25. Casey, B. J., Tottenham, N., Liston, C. & Durston, S. Imaging the developing brain: what have we learned about cognitive development? *Trends Cogn. Sci.* **9**, 104–110 (2005).
26. Hursh, J. B. Conduction velocity and diameter of nerve fibers. *Am. J. Physiol.* **127**, 131–139 (1939).
27. Gerstner, W., Kistler, W.M., Naud, R. & Paninski, L. *Neuronal Dynamics: From Single Neurons to Networks and Models of Cognition* (Cambridge University Press, 2014).#p[;
28. Paus, T., Keshavan, M. & Giedd, J. N. Why do many psychiatric disorders emerge during adolescence? *Nat. Rev. Neurosci.* **9**, 947–957 (2008).
29. Yap, Q. J. et al. Tracking cerebral white matter changes across the lifespan: insights from diffusion tensor imaging studies. *J. Neural Transm.* **120**, 1369–1395 (2013).
30. Geeraert, B. L., Lebel, R. M. & Lebel, C. A multiparametric analysis of white matter maturation during late childhood and adolescence. *Hum. Brain Mapp.* **40**, 4345–4356 (2019).
31. Beck, D. et al. White matter microstructure across the adult lifespan: a mixed longitudinal and cross-sectional study using advanced diffusion models and brain-age prediction. *Neuroimage* **224**, 117441 (2021).

Publisher's note Springer Nature remains neutral with regard to jurisdictional claims in published maps and institutional affiliations.

Open Access This article is licensed under a Creative Commons Attribution 4.0 International License, which permits use, sharing, adaptation, distribution and reproduction in any medium or format, as long as you give appropriate credit to the original author(s) and the source, provide a link to the Creative Commons license, and indicate if changes were made. The images or other third party material in this article are included in the article's Creative Commons license, unless indicated otherwise in a credit line to the material. If material is not included in the article's Creative Commons license and your intended use is not permitted by statutory regulation or exceeds the permitted use, you will need to obtain permission directly from the copyright holder. To view a copy of this license, visit http://creativecommons.org/licenses/by/4.0/.

© The Author(s) 2023

Methods

Subjects

All subjects who underwent epilepsy surgery in the University Medical Center (UMC) Utrecht between 2008 and 2020 were included in a retrospective epilepsy surgery database[32], with approval of the Medical Research Ethical Committee of UMC Utrecht. For subjects included between January 2008 and December 2017, the Medical Research Ethical Committee waived the need for informed consent. Since January 2018, we explicitly ask subjects for informed consent to collect their data for research purposes. No statistical methods were used to predetermine sample sizes and we included all subjects who underwent single-pulse electrical stimulation for clinical purposes during the intracranial grid monitoring period between 2012 and 2020 and met inclusion criteria. Subjects were not provided with compensation. In total, 74 subjects were included in this study (median age 17 years (4–51 years), 38 females), thus spanning age ranges from childhood (6–13 years), adolescence (14–18 years), young adult (19–33 years) and middle age (49–64 years)[33]. Inclusion criteria were the absence of large brain lesions and that electrode positions could be determined based on a computed tomography scan coregistered with a T1 MRI[34]. After electrode localization, electrodes were labeled according to the Freesurfer based Destrieux atlas segmentation[35,36]. The electrodes were well distributed across the age groups (Supplementary Fig. 9). For visualization, the individual subject's electrode positions were converted to Montreal Neurological Institute (MNI)152 space. During the evaluation for epilepsy, the seizure onset zone and eloquent cortex are delineated and a resection area suggested to the surgeon. No different experimental conditions were applied to the subjects and randomization was not possible. Data collection and analysis were not performed blind to the conditions of the experiments.

All CCEPs were reviewed and 4 runs with incorrect stimulation onsets were removed. Furthermore, electrodes that overlapped with another grid, were located on small structural abnormalities or had excessive noise were excluded from analyses. On average, across all subjects, 6.3% of electrodes were excluded. We additionally excluded stimulation pairs that introduced baseline offsets on many measured channels. To ensure that the epilepsy did not affect the result in a systematic manner, the seizure onset zone was annotated in 30 subjects by a clinical neurophysiologist. This allowed comparison of latencies in and outside of the seizure onset region (Supplementary Figs. 6 and 7).

Acquisition

Long-term ECoG data were recorded with subdural electrode grids and strips of 4.2 mm^2 contact surface and an interelectrode distance of 1 cm (Ad-Tech and PMT). Additional depth electrodes were implanted in several subjects but are not included in analyses because they were typically placed in lesions visible on an MRI. Single-pulse electrical stimulation was performed during ECoG recordings with data sampled at 2,048 Hz using a MicroMed LTM64/128 express electroencephalography headbox with integrated programmable stimulator (MicroMed). The stimulation onset was determined accurately by MicroMed hardware, but we note that electrical stimulation creates an artifact from about −9 ms to 9 ms around stimulation onset as channels are coupled to the ground during stimulation. Ten monophasic stimuli with a pulse width of 1 ms were applied at a frequency of 0.2 Hz to two adjacent electrodes. Polarity was alternated after five pulses in 27 of the subjects such that stimulation artifacts are reduced by averaging. A current intensity of 8 mA was used, but in case electrodes were located near central nerves or in the primary sensorimotor cortex, the intensity was lowered to 4 mA to avoid pain or twitches. Changes in amplitude did not systematically influence the results (Supplementary Fig. 1).

N1 latency calculation

To estimate conduction delays across different connections, we calculated the latency of the earliest surface negative deflection in the CCEP in 9–100 ms after stimulation. This response is also referred to as the N1 and is thought to be generated by synchronized, excitatory synaptic activation of the distal layer apical dendrites of the pyramidal cells[20,22] and spread through white matter[19,37]. For each electrode, ten epochs with a time window of 2 s prestimulus to 3 s poststimulus, time-locked to the stimulus, are corrected for baseline (median signal in a time window of 900 ms before stimulation (−1 s to −0.1 s) and averaged for each stimulus pair[38]. For each averaged epoch, the median is subtracted (−2 s to −0.1 s), and the s.d. is calculated in this prestimulus window. N1s are detected when the evoked response exceeds 3.4 × s.d. in a time window of 9–100 ms poststimulation, excluding earlier times due to potential stimulation artifacts.

Stimulation artifacts can potentially spread to nearby electrodes through volume conduction and the following helped ensure that this did not affect our results. First, volume conduction effects are largest in the first 1–8 ms after electrical stimulation[39], and N1 detection was done after this time, from 9 to 100 ms. Second, we excluded electrodes within 13 mm from the stimulated electrode pair, at which distance the effects of volume conduction are largely negligible[40]. Lastly, in a previous manuscript using a subset of these data, we ensured that volume conduction did not play an important role by showing that the latencies differ across measured electrodes for a single stimulated pair[41]. We apply a similar method and show in Supplementary Fig. 8 that the detected N1 latencies varied across measured electrodes.

While the CCEP waveform has more complex features, the N1 component is the most robust and relevant feature to answer questions about direct electrical conduction[18]. The N1 is measured robustly with ECoG at the brain surface and can be detected as early as 10 ms after stimulation onset. The N1 has been related to direct cortico-cortical connections in many other CCEP studies of, for example, the motor system[42], cingulum bundle[43,44], frontal aslant tract[45] and the superior longitudinal fasciculus[46]. Moreover, previous studies showed that the N1 corresponds relatively well with diffusion-MRI-derived white matter endpoints[47], the N1 latency relates linearly with the distance traveled along a fiber bundle[48,49] and that the N1 propagation velocity correlates with fractional anisotropy in the white matter[37].

Integrating electrode locations with a white matter atlas

The connectivity between the frontal, temporal, parietal and pre/postcentral (primary sensorimotor) areas was investigated based on the AF, the SLF and TPAT. We focus on these connections, and exclude connections to regions without sufficient electrode coverage for across-subject correlations, such as the occipital lobe. Each of these tracts was defined based on the population-averaged tractography atlases HCP1065 (AF, SLF, TPAT)[23] and HCP842 (U-fibers)[50]. The SLF was split into two sections connecting frontal and parietal and frontal and central brain regions, because merging these sections would lead to inaccurate estimates of the length of the SLF and bias transmission speed estimates described in the next section. We subsequently matched the ECoG electrodes, located on the gray matter surface, to the tractography atlas using the gray matter endpoint probability estimates of the tracts[23]. In this way, we were able to investigate the CCEP based connectivity for different fiber tracts.

Transmission speed estimation

To estimate the transmission speed along the tracts, we calculated the tract length in each subject. Using ANTs registration implemented in lead-dbs[51] between the subject MRI and MNI space, the tracts from the atlases were registered to the native space of each subject. In each subject's native space, the length of each tract was then calculated by taking the average length over all tract fibers in native space. To estimate transmission speed, the latency of each CCEP along a specific tract was divided by the respective length of the tract to obtain a speed in meters per second.

Statistics

To describe the relationship between age and conduction delay and/or age and transmission speed, we fit a first- and second-order polynomial model where age predicts the N1 latency or the transmission speed. These models have been used before in MRI studies to characterize development-related changes in gray and white matter properties[6,52]. Fitting these models with leave-one-out cross-validation lets the data indicate whether the development of different connections is better described by a linear model or a quadratic model with a local minimum. To ensure that certain datapoints with high leverage did not unduly influence the results, we performed a robust regression with bisquare weight function and a tuning constant of 4.685. Data distribution was assumed to be normal but this was not formally tested. The coefficient of determination (R^2) was used to indicate how well the model described the data:

$$R^2 = 1 - \frac{SS_{res}}{SS_{tot}}$$

in which

$$SS_{res} = \sum_i (y_i - f_i)^2 \text{ and } SS_{tot} = \sum_i (y_i - \bar{y})^2.$$

We note that the R^2 provides the explained variance relative to a baseline model that predicts the average $\bar{y}$. If the model predicts the data better than baseline, R^2 will be larger than 0, if the model predicts the data worse than baseline, R^2 can be smaller than 0. The R^2 therefore indicates how much of the variance in latency is predicted by age as compared with no change with age. When necessary, statistical tests were corrected for multiple comparisons using a false discovery rate (FDR) correction.

Reporting summary

Further information on research design is available in the Nature Portfolio Reporting Summary linked to this article.

Data availability

The data that support the findings of this study are being made available in BIDS format on OpenNeuro: https://openneuro.org/datasets/ds004080. Atlases of white matter tracts were defined based on the population-averaged tractography atlases HCP1065 (AF, SLF, TPAT)[23] and HCP842 (U-fibers)[50]: https://brain.labsolver.org/hcp_trk_atlas.

Code availability

The code to analyze the data and generate all figures of this manuscript is available on GitHub: https://github.com/MultimodalNeuroimagingLab/mnl_ccepBids.

References

32. Demuru, M. et al. A practical workflow for organizing clinical intraoperative and long-term iEEG data in BIDS. *Neuroinformatics* **20.3**, 727–736 (2022).
33. Geifman, N., Cohen, R. & Rubin, E. Redefining meaningful age groups in the context of disease. *Age* **35**, 2357–2366 (2013).
34. Hermes, D., Miller, K. J., Noordmans, H. J., Vansteensel, M. J. & Ramsey, N. F. Automated electrocorticographic electrode localization on individually rendered brain surfaces. *J. Neurosci. Methods* **185**, 293–298 (2010).
35. Destrieux, C., Fischl, B., Dale, A. & Halgren, E. Automatic parcellation of human cortical gyri and sulci using standard anatomical nomenclature. *Neuroimage* **53**, 1–15 (2010).
36. Fischl, B. et al. Automatically parcellating the human cerebral cortex. *Cereb. Cortex* **14**, 11–22 (2004).
37. Silverstein, B. H. et al. Dynamic tractography: Integrating cortico-cortical evoked potentials and diffusion imaging. *Neuroimage* **215**, 116763 (2020).
38. van Blooijs, D., Leijten, F. S. S., van Rijen, P. C., Meijer, H. G. E. & Huiskamp, G. J. M. Evoked directional network characteristics of epileptogenic tissue derived from single pulse electrical stimulation. *Hum. Brain Mapp.* **39**, 4611–4622 (2018).
39. Trebaul, L. et al. Stimulation artifact correction method for estimation of early cortico-cortical evoked potentials. *J. Neurosci. Methods* **264**, 94–102 (2016).
40. Prime, D., Woolfe, M., O'Keefe, S., Rowlands, D. & Dionisio, S. Quantifying volume conducted potential using stimulation artefact in cortico-cortical evoked potentials. *J. Neurosci. Methods* **337**, 108639 (2020).
41. Hebbink, J. et al. A comparison of evoked and non-evoked functional networks. *BrainTopogr.* **32**, 405–417 (2019).
42. Matsumoto, R. et al. Functional connectivity in human cortical motor system: a cortico-cortical evoked potential study. *Brain* **130**, 181–197 (2007).
43. Kubota, Y. et al. In vivo human hippocampal cingulate connectivity: a corticocortical evoked potentials (CCEPs) study. *Clin. Neurophysiol.* **124**, 1547–1556 (2013).
44. Oane, I. et al. Cingulate cortex function and multi-modal connectivity mapped using intracranial stimulation. *Neuroimage* **220**, 117059 (2020).
45. Yang, H.-R., Ra, Y.-S. & Koo, Y. S. Intraoperative monitoring of cortico-cortical evoked potentials of the frontal aslant tract in a patient with oligodendroglioma. *Ann. Clin. Neurophysiol.* **24**, 21–25 (2022).
46. Matsumoto, R. et al. Parieto-frontal network in humans studied by cortico-cortical evoked potential. *Hum. Brain Mapp.* **33**, 2856–2872 (2012).
47. Adkinson, J. A. et al. Imaging versus electrographic connectivity in human mood-related fronto-temporal networks. *Brain Stimul.* **15**, 554–565 (2022).
48. Trebaul, L. et al. Probabilistic functional tractography of the human cortex revisited. *Neuroimage* **181**, 414–429 (2018).
49. Matsumoto, R., Kunieda, T. & Nair, D. Single pulse electrical stimulation to probe functional and pathological connectivity in epilepsy. *Seizure* **44**, 27–36 (2017).
50. Yeh, F.-C. et al. Population-averaged atlas of the macroscale human structural connectome and its network topology. *Neuroimage* **178**, 57–68 (2018).
51. Horn, A. & Kühn, A. A. Lead-DBS: a toolbox for deep brain stimulation electrode localizations and visualizations. *Neuroimage* **107**, 127–135 (2015).
52. Giedd, J. N. et al. Brain development during childhood and adolescence: a longitudinal MRI study. *Nat. Neurosci.* **2**, 861–863 (1999).

Acknowledgements

We thank the SEIN-UMCU RESPect database group (C.J.J. van Asch, L. van de Berg, S. Blok, M.D. Bourez, K.P.J. Braun, J.W. Dankbaar, C.H. Ferrier, T.A. Gebbink, P.H. Gosselaar, M.G.G. Hobbelink, F.W.A. Hoefnagels, N.E.C. van Klink, M.A. van 't Klooster, G.A.P. de Kort, M.H.M. Mantione, A. Muhlebner, J.M. Ophorst, R. van Regteren, P.C. van Rijen, S.M.A. van der Salm, E.V. Schaft, M.M.J. van Schooneveld, H. Smeding, D. Sun, A. Velders, M.J.E. van Zandvoort, G.J.M. Zijlmans, E. Zuidhoek and J. Zwemmer) for their contributions and help in collecting the data, and G. Ojeda Valencia for proofreading the manuscript. Research reported in this publication was supported by the National Institute of Mental Health of the National Institutes of Health under Award Number R01MH122258 (D.H. and F.S.S.L.), the content is solely the responsibility of the authors and does not necessarily represent the official views of the National Institutes of Health, the EpilepsieNL under Award Number

NEF17-07 (D.v.B.) and the UMC Utrecht Alexandre Suerman MD/PhD Stipendium 2015 (W.J.E.M.Z.).

Author contributions

D.H., D.v.B. and F.S.S.L. conceived experiments. D.v.B., G.M.H., P.v.E., K.J.M. and F.S.S.L. collected the data and performed the experiments. D.v.B., M.A.v.d.B., J.F.v.d.A., G.M.H., G.C., M.D., W.J.E.M.Z. and D.H. performed the data curation. D.v.B., M.A.v.d.B., G.M.H., M.D., K.J.M. and D.H. contributed tools to curate and analyze data. D.v.B., M.A.v.d.B., J.F.v.d.A. and D.H. analyzed the data. The original draft was written by D.v.B. and D.H. and was revised by and edited by all authors. D.H. and F.S.S.L supervised the project.

Competing interests

The authors declare no competing interests.

Additional information

Supplementary information The online version contains supplementary material available at https://doi.org/10.1038/s41593-023-01272-0.

Correspondence and requests for materials should be addressed to Dora Hermes.

Peer review information *Nature Neuroscience* thanks Michael Cohen, Jason Yeatman and the other, anonymous reviewer(s) for their contribution to the peer review of this work.

Reprints and permissions information is available at www.nature.com/reprints.

nature portfolio

Corresponding author(s): Dora Hermes

Last updated by author(s): 2022/03/22

Reporting Summary

Nature Portfolio wishes to improve the reproducibility of the work that we publish. This form provides structure for consistency and transparency in reporting. For further information on Nature Portfolio policies, see our Editorial Policies and the Editorial Policy Checklist.

Statistics

For all statistical analyses, confirm that the following items are present in the figure legend, table legend, main text, or Methods section.

n/a	Confirmed	
☐	☒	The exact sample size (*n*) for each experimental group/condition, given as a discrete number and unit of measurement
☐	☒	A statement on whether measurements were taken from distinct samples or whether the same sample was measured repeatedly
☐	☒	The statistical test(s) used AND whether they are one- or two-sided *Only common tests should be described solely by name; describe more complex techniques in the Methods section.*
☐	☒	A description of all covariates tested
☐	☒	A description of any assumptions or corrections, such as tests of normality and adjustment for multiple comparisons
☐	☒	A full description of the statistical parameters including central tendency (e.g. means) or other basic estimates (e.g. regression coefficient) AND variation (e.g. standard deviation) or associated estimates of uncertainty (e.g. confidence intervals)
☐	☒	For null hypothesis testing, the test statistic (e.g. *F*, *t*, *r*) with confidence intervals, effect sizes, degrees of freedom and *P* value noted *Give P values as exact values whenever suitable.*
☒	☐	For Bayesian analysis, information on the choice of priors and Markov chain Monte Carlo settings
☒	☐	For hierarchical and complex designs, identification of the appropriate level for tests and full reporting of outcomes
☐	☒	Estimates of effect sizes (e.g. Cohen's *d*, Pearson's *r*), indicating how they were calculated

Our web collection on statistics for biologists contains articles on many of the points above.

Software and code

Policy information about availability of computer code

Data collection	No software was used for data collection.
Data analysis	For segmenting the imaging data we used Freesurfer V6.0. We used ANTs registration in lead-dbs V1.6.3 to register white matter atlases to the native space of each subject. The Matlab code to analyze the data and generate all figures of this manuscript is available on GitHub: https://github.com/MultimodalNeuroimagingLab/mnl_ccepBids and is tested with Matlab versions 2021a and 2022a.

For manuscripts utilizing custom algorithms or software that are central to the research but not yet described in published literature, software must be made available to editors and reviewers. We strongly encourage code deposition in a community repository (e.g. GitHub). See the Nature Portfolio guidelines for submitting code & software for further information.

Data

Policy information about availability of data

All manuscripts must include a data availability statement. This statement should provide the following information, where applicable:

- Accession codes, unique identifiers, or web links for publicly available datasets
- A description of any restrictions on data availability
- For clinical datasets or third party data, please ensure that the statement adheres to our policy

The data that support the findings of this study are being made available in BIDS format on OpenNeuro: https://openneuro.org/datasets/ds004080. Identifiers are removed from the data and electrode positions with anatomical Destrieux atlas labels are shared in MNI152 space to remove the need for sharing MRI scans. Atlases of white matter tracts were defined based on the population-averaged tractography atlasses HCP1065 (AF, SLF, TPAT) and HCP842 (U-fibers): https://brain.labsolver.org/hcp_trk_atlas.

Field-specific reporting

Please select the one below that is the best fit for your research. If you are not sure, read the appropriate sections before making your selection.

☒ Life sciences ☐ Behavioural & social sciences ☐ Ecological, evolutionary & environmental sciences

For a reference copy of the document with all sections, see nature.com/documents/nr-reporting-summary-flat.pdf

Life sciences study design

All studies must disclose on these points even when the disclosure is negative.

Sample size	No statistical methods were used to pre-determine sample sizes and we included all subjects who underwent Single Pulse Electrical Stimulation (SPES) for clinical purposes during the intracranial grid monitoring period between 2012 and 2020 and met inclusion criteria, resulting in 74 subjects included in the study. For these subjects, we analyzed connections where at least 20 subjects had electrodes on both endpoints, and exclude connections to regions without sufficient electrode coverage for across-subject correlations, such as the occipital lobe. A retrospective power analysis with an expected Pearson correlation of .60, a=.05, and desired power of 80%, tells us a sample size of at least 19 is desirable.
Data exclusions	Subjects who underwent epilepsy surgery in the UMC Utrecht between 2008 and 2020, underwent single pulse electrical stimulation and did not have large structural abnormalities were included in analyses. Standard, pre-established criteria were used to review iEEG data: electrodes and data segments with excessive noise were annotated in the data (following BIDS structure) and are excluded from analyses. Stimulation pairs that introduced baseline offsets on many measured channels were additionally excluded from all analyses.
Replication	We did not include multiple groups to replicate results.
Randomization	There were no experimental groups.
Blinding	Subjects were not assigned to groups.

Reporting for specific materials, systems and methods

We require information from authors about some types of materials, experimental systems and methods used in many studies. Here, indicate whether each material, system or method listed is relevant to your study. If you are not sure if a list item applies to your research, read the appropriate section before selecting a response.

Materials & experimental systems

n/a	Involved in the study
☒	☐ Antibodies
☒	☐ Eukaryotic cell lines
☒	☐ Palaeontology and archaeology
☒	☐ Animals and other organisms
☐	☒ Human research participants
☒	☐ Clinical data
☒	☐ Dual use research of concern

Methods

n/a	Involved in the study
☒	☐ ChIP-seq
☒	☐ Flow cytometry
☒	☐ MRI-based neuroimaging

Human research participants

Policy information about studies involving human research participants

Population characteristics	This study includes 74 subjects who underwent epilepsy surgery in the UMC Utrecht between 2008 and 2020, the median age was 17 years (range 4-51 years), there were 38 females.
Recruitment	The study was partially retrospective (before 2018), with IRB permission. After 2018, subjects undergoing epilepsy monitoring and single pulse electrical stimulation for clinical purposes were asked for informed consent to include their data for research purposes. Recruitment may therefore include biases from this population, which we address in the manuscript.
Ethics oversight	Medical Research Ethical Committee from the UMC Utrecht

Note that full information on the approval of the study protocol must also be provided in the manuscript.